The Cosmic Origins Spectrograph: NUV Imaging Performance

Paul Goudfrooij[1], E. Burgh[2], A. Aloisi[1], C. Keyes[1], D. Sahnow[3], S. Penton[2], STScI COS Team, and COS IDT Team
[1]STScI, [2]University of Colorado, [3]Johns Hopkins University

ABSTRACT

We describe the COS NUV imaging performance as derived from data taken during the Observatory Verification period after HST Servicing Mission #4. This includes photometric growth curves using data taken with the two available MIRROR settings (MIRRORA and MIRRORB) and the PSA and BOA apertures, throughput and image quality as function of spatial offset from the center of the COS aperture, and a description of the imaging-mode point spread function (PSF). The observed PSF is fully consistent with the model (at good HST focus), except for two minor ghosts located about 20 pixels away from the PSF center. A comparison of imaging observations of a cool and a hot flux standard star reveals a ***significantly higher red sensitivity*** of the COS imaging modes than that predicted from ground calibration data. Apart from that, the results are roughly consistent with predictions from ground calibration. The new throughput curves are used in the COS imaging and imaging target acquisition exposure time calculators since October 7, 2009.

Target Flux Standard Stars

To enable a proper initial on-orbit flux calibration for the COS imaging modes, the targets comprised two HST flux standard stars with widely different spectral energy distributions (SEDs):

1. The solar-type (G2V) star **P330E** for which a high-quality HST reference spectrum is available from 2000–24440 Å (e.g., Bohlin et al. 2006). Numerous images were taken in PSA/MIRRORA mode and 1 deep PSA/MIRRORB image.
2. The DBQ4 star **LDS749B**, a relatively cool white dwarf star with T_{eff} = 13,575 K for which the HST reference spectrum covers 1150 – 24960 Å using STIS and NICMOS data (e.g., Bohlin & Koester 2008). Images were taken using PSA/MIRRORB, BOA/MIRRORA and BOA/MIRRORB modes.

As the short-wavelength cutoff of the throughput curves of both MIRRORA and MIRRORB imaging modes is shortward of the shortest wavelength covered by the P330E reference spectrum, we supplemented the latter in the 1200–2000 Å region by a scaled version of the Solar spectrum of Colina et al. (1996). Note that the radiation of solar-type stars below 2000 Å is dominated by chromospheric emission which undergoes variations associated with the solar activity cycle and rotation period. Variations of up to ±15% are known to occur for the Sun in the 1500 – 2000 Å interval (Woods et al. 1996). However, the low sensitivity of the COS MAMA in this wavelength regime renders the systematic uncertainty caused by this variation negligible in the context of the following photometric analyses. The SEDs of the two targets are shown in Fig. 1.

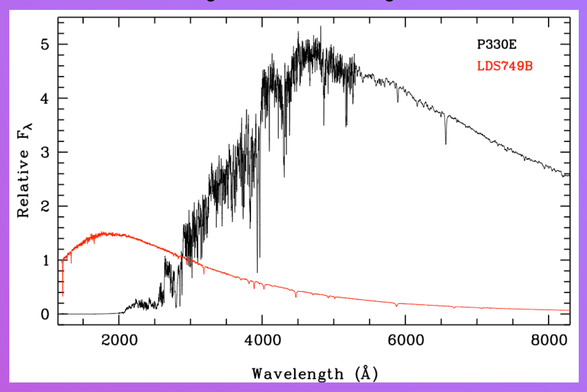

Figure 1. *Spectral Energy Distributions (SEDs) of the two target flux standard stars P330E (black line) and LDS749B (red line). The two SEDs were normalized to unity at a wavelength of 3000 Å to facilitate the comparison.*

The COS Imaging Point Spread Function

We created model imaging-mode PSFs at wavelengths of 170 - 320 nm using steps of 10 nm starting from a ZEMAX model of the HST Optical Mirror Assembly (OTA). This was modified for the COS aperture position using Optical Path Difference info on the HST OTA available within TinyTim and including a 15 nm RMS wave-front error due to zonal errors of the OTA (Krist & Burrows 1995). Finally, the PSF was convolved with the known blur function of the STIS NUV-MAMA (since the COS MAMA is its flight spare).

The main features of the COS PSF are shown in the left-hand panel of Fig. 2 which presents a deep image of P330E taken near perfect HST focus. Note the two low-level "ghost" images located about 20 pixels to the right and upper left from the center of the PSF. The peak intensity of the brightest of the two ghosts is about 0.1% of that of the PSF center. This empirical PSF is compared to the model PSF in the right-hand panel of Fig. 2. For this purpose, the SED of P330E was folded through the throughput curve of the PSA/MIRRORA mode (see "Update to Mirror Throughput Curves" section) to derive weighting factors as a function of wavelength which were then applied to the model PSFs at the various wavelengths. The model PSF is found to provide an excellent description of the empirical PSF except near the radii where the ghosts are located.

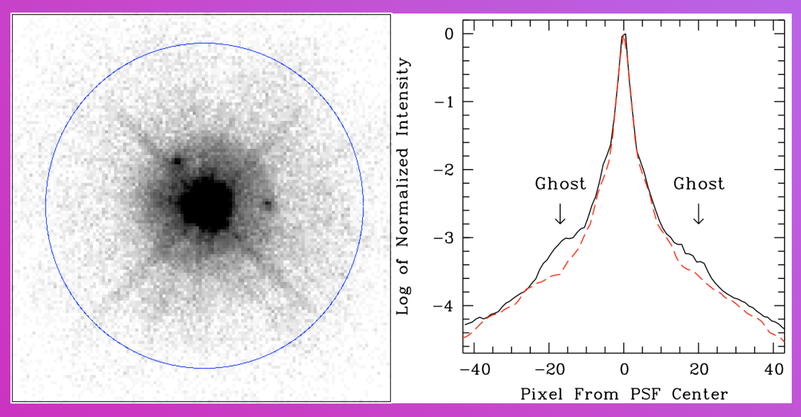

Figure 2. ***Left Panel****: Inner 3x3 arcsec² of deep PSA/MIRRORA image of P330E, plotted with logarithmic intensity scale. The COS aperture (radius of 1.25 arcsec) is shown as a blue circle.* ***Right panel****: Comparison of observed azimuth-averaged PSF (black solid line) with model azimuth-averaged PSF for target P330E in PSA/MIRRORA configuration (red dashed line). The location of the two ghosts (seen in the left panel) are indicated.*

Photometric Analysis

We used the DAOPHOT package as implemented within IRAF for photometric growth curve analysis. For MIRRORA data, aperture photometry was conducted using various aperture radii ranging from 0.5 to 60 pixels. For MIRRORB data, the finite thickness of the order-sorting filter on the mirror causes a secondary image that contains about 45% of the flux in the primary image, located about 20 pixels away from the primary image. Hence the largest aperture radius for MIRRORB data was chosen to be 10 pixels. Target centering was performed using intensity-weighted averages of the x and y profiles. Given the presence of extended wings in the COS NUV point spread function (cf. Fig. 2), the sky background was determined within a circular annulus with an inner radius of 60 pixels and a width of 10 pixels. Results of the growth curve analysis are shown in Fig. 3 for all exposures taken at the center of the COS aperture.

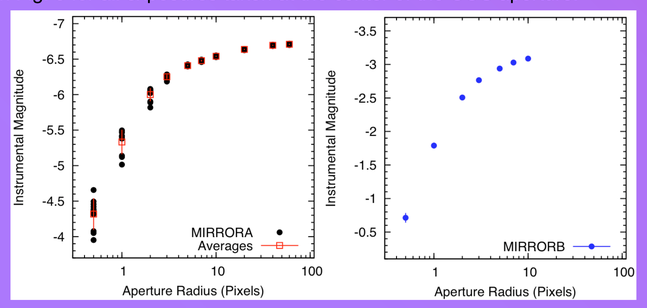

Figure 3. *Photometric growth curve for PSA imaging of target P330E. The left panel shows all individual measurements for MIRRORA in black and average measurements at each aperture radius in red (along with a 1σ error bar for the latter). Note the significant scatter at small aperture radii, which are due to focus variations during the HST orbit (cf. below). The right panel shows the MIRRORB measurements along with their (very small) 1σ Poisson uncertainties (only one image was taken in MIRRORB). Both panels use the same relative scale in the ordinate to facilitate direct comparison.*

PSF Size versus HST Focus

To investigate the influence of the HST focus in the context of the observed scatter in the photometry through small measurement apertures, we had the Telescopes Group at STScI create a focus model simulation for the optical telescope assembly (OTA) of the HST during the orbits in which the exposures shown in Fig. 3 were taken. The focus values are plotted as a function of time in Fig. 4 along with measured FWHM values of the images (using a 2-D Gaussian fit). Note the clear relation between the focus and the FWHM values, even though there are a few outliers. A linear fit between FWHM and focus values yields a RMS error of only 0.10 pixels.

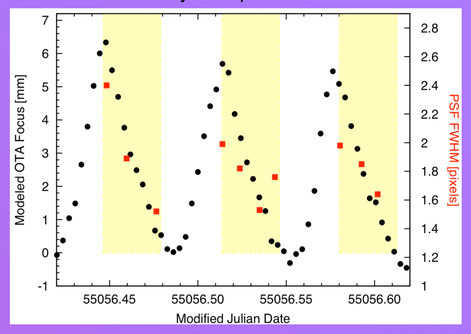

Figure 4. *The relation between HST focus values and COS PSF size during the observations. Black circles represent simulated HST OTA focus values (see values on left-hand ordinate) while red squares represent PSF FWHM measurements at the center of the COS aperture (see right-hand ordinate). The time intervals shaded in yellow indicate the parts of the HST orbits during which the observations occurred.*

Throughput as Function of Position within Aperture

Due to the combination of the wide wings of the COS PSF and the size of the PSA aperture (radius of 1.25 arcsec), the light received from a point source gets diminished when the target is placed away from the center of the aperture. See Fig. 5 below.

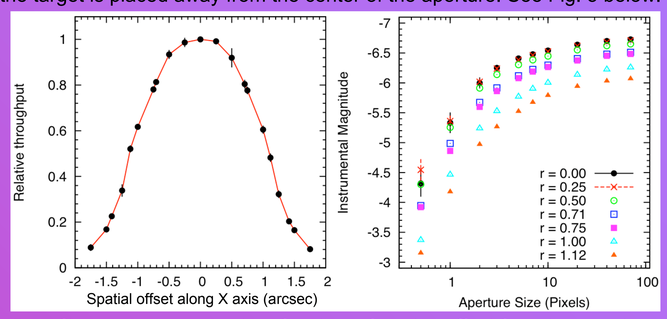

Figure 5. ***Left panel****: Throughput as function of spatial offset from the aperture center. This figure was derived by averaging several measurements over 180° of azimuth.* ***Right panel****: Photometric growth curve for PSA/MIRRORA as function of spatial offset from the aperture center (see legend for the different symbols). Error bars are plotted only for the two innermost positions for clarity considerations.*

Update to COS Mirror Throughput Curves

Total count rates found for P330E and LDS749B in the PSA/MIRRORB configuration were compared with predictions based on ground calibration. The ratio of observed to predicted count rates was found to be significantly higher for P330E than for LDS749B, an 8σ effect (1.031 ± 0.011 vs. 0.946 ± 0.006). Since P330E has a much "redder" SED than LDS749B, this indicates a ***higher red sensitivity*** than that given by the pre-flight throughput curves.

Revised throughput curves were determined as follows. Between 1248 and 2998 Å, the shapes of the pre-flight curves were directly adopted as they were determined from sensitive Thermal Vacuum measurements. For wavelengths longer than 2998 Å, we multiplied the pre-flight throughput curves of MIRRORA and MIRRORB by a wavelength-dependent scale factor that is unity at 2998 Å and has a spectral shape that yields a count rate ratio for P330E vs. LDS749B which is equal to the observed ratio. The new throughput curves were implemented in **`synphot`** on 10/07/09 and are depicted in Fig. 6.

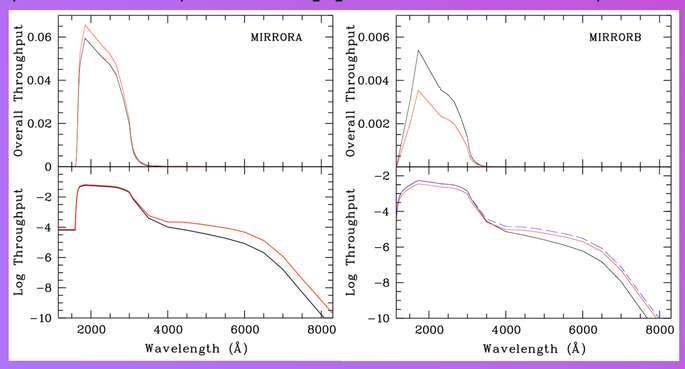

Figure 6. ***Left Panel:*** *The black line shows the pre-flight throughput curve for the COS PSA/MIRRORA mode, while the red line shows the newly derived throughput curve (see text above).* ***Right Panel:*** *Same as left panel, but for PSA/MIRRORB mode. Note the significantly lower throughput values for λ < 2998 Å in the new throughput curve, which is due to the fact that the pre-flight values included the secondary peak in MIRRORB images whereas the new curve does not. The curves shown here are end-to-end throughputs for COS, but do not include the contribution from the HST OTA.*

Image Drift During 5 HST Orbits

Pre-flight tests of COS showed some drift of the Optical Select Mirrors (OSMs) after they were stopped in their nominal positions. As this affects imaging observations as well as spectroscopic ones, we quantified this drift during in-flight tests using several WCA (wavelength calibration aperture) exposures. The result is depicted in Fig. 7. The majority of the drift is in X (~3.5 pixels max), and most likely due to settling of the grating/mirror rotation mechanism. As seen in Fig. 7, the drift is well fit with an exponential decay giving a characteristic size and time scale (one for each OSM). ***Observers using imaging exposures with exp. times longer than ~200 s are urged to use the TIME-TAG operating mode with the FLASH optional parameter*** *(see phase II proposal instructions)*, which takes short WCA flashes during an exposure, enabling one to follow the drift accurately. This will allow one to retain the excellent COS NUV imaging performance during long exposures.

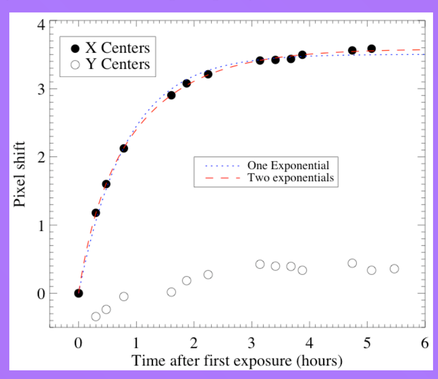

Figure 7. *Image drift in X and Y as function of time (see legend for symbols). The drift is well-fit by a (double) exponential curve. The fit in the X direction is shown by dotted and dashed lines.*

Final Note

This poster is a preview summary of a forthcoming COS Instrument Science Report (Goudfrooij et al. 2010) which will contain much more detail and quantitative information.

References

Bohlin, R. C., Riess, A., & de Jong, R., 2006, NICMOS Instrument Science Report 2006-002 (Baltimore: STScI)

Bohlin, R. C., & Koester, D., 2008, AJ, **135**, 1092

Colina, L., Bohlin, R. C., & Castelli, F., 1996, AJ, **112**, 307

Goudfrooij, P., Burgh, E., Aloisi, A., Hartig. G., & Penton, S. 2010, COS Instrument Science Report, *in preparation*

Krist, J. E., & Burrows, C. J. 1995, "Phase-retrieval Analysis of Pre-and Post-repair Hubble Space Telescope Images", Applied Optics, **34**, 4951